mRNA adenosine methylase (MTA) deposits m^{6}A on pri-miRNAs to modulate miRNA biogenesis in *Arabidopsis thaliana*

Susheel Sagar Bhat[a,1], Dawid Bielewicz[a,1], Tomasz Gulanicz[a,b], Zsuzsanna Bodi[c], Xiang Yu[d], Stephen J. Anderson[d], Lukasz Szewc[a], Mateusz Bajczyk[a], Jakub Dolata[a], Natalia Grzelak[a], Dariusz J. Smolinski[b,e], Brian D. Gregory[d], Rupert G. Fray[c], Artur Jarmolowski[a,2], and Zofia Szweykowska-Kulinska[a,2]

[a]Department of Gene Expression, Institute of Molecular Biology and Biotechnology, Faculty of Biology, Adam Mickiewicz University, 61-614 Poznan, Poland; [b]Centre For Modern Interdisciplinary Technologies, Nicolaus Copernicus University, 87-100 Torun, Poland; [c]School of Biosciences, Plant Science Division, University of Nottingham, Sutton Bonington, Loughborough LE12 5RD, United Kingdom; [d]Department of Biology, University of Pennsylvania, Philadelphia, PA 19104; and [e]Department of Cellular and Molecular Biology, Nicolaus Copernicus University, 87-100 Torun, Poland

Edited by David C. Baulcombe, University of Cambridge, Cambridge, United Kingdom, and approved July 27, 2020 (received for review February 27, 2020)

In *Arabidopsis thaliana*, the METTL3 homolog, mRNA adenosine methylase (MTA) introduces N^6-methyladenosine (m^{6}A) into various coding and noncoding RNAs of the plant transcriptome. Here, we show that an MTA-deficient mutant (*mta*) has decreased levels of microRNAs (miRNAs) but accumulates primary miRNA transcripts (pri-miRNAs). Moreover, pri-miRNAs are methylated by MTA, and RNA structure probing analysis reveals a decrease in secondary structure within stem–loop regions of these transcripts in *mta* mutant plants. We demonstrate interaction between MTA and both RNA Polymerase II and TOUGH (TGH), a plant protein needed for early steps of miRNA biogenesis. Both MTA and TGH are necessary for efficient colocalization of the Microprocessor components Dicer-like 1 (DCL1) and Hyponastic Leaves 1 (HYL1) with RNA Polymerase II. We propose that secondary structure of miRNA precursors induced by their MTA-dependent m^{6}A methylation status, together with direct interactions between MTA and TGH, influence the recruitment of Microprocessor to plant pri-miRNAs. Therefore, the lack of MTA in *mta* mutant plants disturbs pri-miRNA processing and leads to the decrease in miRNA accumulation. Furthermore, our findings reveal that reduced miR393b levels likely contributes to the impaired auxin response phenotypes of *mta* mutant plants.

miRNA biogenesis | MTA | m^{6}A methylation

One of the most abundant mRNA modifications in eukaryotic cells, N^6-methyladenosine (m^{6}A), can regulate eukaryote gene expression at co- as well as posttranscriptional levels. m^{6}A methylation in animal mRNAs is associated with several biological processes, ranging from cell development (1, 2) to carcinogenesis (3) and viral infections (4, 5), with the underpinning mechanisms including m^{6}A regulated pre-mRNA splicing patterns, mRNA export, mRNA stability, and changes in translational efficiency (1). A group of proteins that collectively form the RNA methylation "writer" complex have been characterized and are well conserved between plants and animals. The mammalian m^{6}A methyltransferase complex consists of methyltransferase-like 3 (METTL3) (2), methyltransferase-like 14 (METTL14) (6), Wilms' tumor 1-associating protein (WTAP) (7), VIRMA (KIAA1429) (8), RNA-binding motif protein 15 (RBM15) (9), and zinc finger CCCH-type Containing 13 (ZC3H13) (10, 11). While METTL3 has been identified as the catalytic protein in this complex (2), auxiliary proteins provide specificity and help with proper localization of the complex (1). The m^{6}A mark can be recognized by various "readers," the best-characterized of which belong to the YT521-B homology (YTH) domain family (12–15). The modification can also be removed from transcripts by "erasers," which in humans include the fat mass and obesity-associated protein (16) and α-ketoglutarate-dependent dioxygenase alkB homolog 5 (ALKBH5) (17).

In *Arabidopsis thaliana*, the presence of m^{6}A was first reported in 2008 and was shown to be dependent upon the activity of mRNA adenosine methylase A (MTA; a homolog of human METTL3), the catalytic component of *Arabidopsis* m^{6}A methyltransferase complex (18). FKBP12 interacting protein 37 kDa (FIP37, a homolog of WTAP) was the first identified methyltransferase-interacting complex member in eukaryotes (18). Later, FIP37 was further characterized and shown to be required for m^{6}A formation in mRNA (19). Other protein components of the plant m^{6}A methyltransferase complex that have been identified include: MTB (methytransferase B, a homolog of METTL14), VIR (Virilizer, a homolog of VIRMA), and *At*HAKAI (a homolog of HAKAI) (20). In *Arabidopsis*, evolutionarily conserved C-terminal region proteins are the orthologs of the mammalian YTH family of proteins and are the only plant readers that have been identified so far (21–23). ALKBH10B and

Significance

Recently N^6-methyladenosine (m^{6}A) methylation has emerged as a biological process with significant impact on cellular functions. However, almost all the research regarding m^{6}A methylation has been based on mRNAs. In our research, we focus on how m^{6}A methylation affects microRNA (miRNA) biogenesis in *Arabidopsis*. In brief, we show that m^{6}A methylation is necessary to maintain proper levels of mature miRNAs as well as their precursors. m^{6}A mark affects pri-miRNA secondary structures and affects the recruitment of the Microprocessor to pri-miRNAs. We also demonstrate the interactions of MTA (m^{6}A writer) with other proteins involved in miRNA biogenesis, namely RNA Polymerase II and TOUGH. Our study provides evidence of the role played by m^{6}A in plant miRNA biogenesis.

Author contributions: A.J. and Z.S.-K. conceived the idea and designed research; S.S.B. and D.B. participated in experimental design; S.S.B., D.B., T.G., Z.B., X.Y., S.J.A., L.S., M.B., J.D., N.G., D.J.S., B.D.G., and R.G.F. performed research; S.S.B., D.B., X.Y., S.J.A., L.S., M.B., J.D., B.D.G., R.G.F., A.J., and Z.S.-K. analyzed data; and S.S.B., D.B., D.J.S., B.D.G., A.J., and Z.S.-K. wrote the paper.

The authors declare no competing interest.

This article is a PNAS Direct Submission.

[1]S.S.B. and D.B. contributed equally to this work.

[2]To whom correspondence may be addressed. Email: artjarmo@amu.edu.pl or zofszwey@amu.edu.pl.

This article contains supporting information online at https://www.pnas.org/lookup/suppl/doi:10.1073/pnas.2003733117/-/DCSupplemental.

First published August 17, 2020.

ALKBH9B represent the characterized *Arabidopsis* m^{6}A erasers (24, 25).

Null mutants of MTA or any other members of the core writer complex (i.e., MTB, FIP37, and VIR) are embryo-lethal (18–20), indicating an essential function for this modification. However, hypomorphic knockdown mutants of these writers have been obtained and typically show an 80 to 90% reduction in m^{6}A levels (19, 20, 26). In contrast, reader and eraser knockouts are viable (23–25). Studies utilizing these various mutant plant lines indicate a role of this modification in embryogenesis, proper plant development (trichome morphology, meristem maintenance, vascular development), flowering time and flower morphology, and pathogen response (18–20, 24–26).

Many aspects of plant development and metabolism are controlled by microRNAs (miRNAs), and the complex phenotypes of low methylation plants have aspects reminiscent of miRNA biogenesis pathway mutants (see ref. 27 for review) and might be, at least partially, explained by the influence of m^{6}A on miRNA biogenesis. miRNAs are small endogenous noncoding RNAs that are ∼21 nt in length and are important players in regulating cellular metabolism. miRNAs are derived from hairpins present in primary miRNAs (pri-miRNAs) that are synthetized by RNA Polymerase II (RNA Pol II), and further processed by RNase III-type enzymes associated with and assisted by other proteins. In animals, where m^{6}A is important for biogenesis of many miRNAs, m^{6}A plays the role of a mark, identified by a reader protein (heterogeneous nuclear ribonucleoprotein A2/B1; HNRNPA2B1) that facilitates the recruitment of downstream enzymes and associated proteins to pri-miRNAs, thus facilitating their processing to miRNAs. Accordingly, it was shown that depletion of METTL3 leads to decreased accumulation of miRNAs and to an overaccumulation of pri-miRNAs due to their impaired processing (28, 29). While most of the findings related to m^{6}A in plants concern mRNAs, its role in miRNA biogenesis in plants remains unknown.

In this study, we provide evidence that biogenesis of at least 25% of *Arabidopsis* miRNAs is affected by the absence of the m^{6}A mark. We show that plant pri-miRNAs are m^{6}A-methylated by MTA, and deficiency of MTA (and thus m^{6}A) leads to accumulation of pri-miRNAs accompanied by lower miRNA levels. We also show that MTA interacts with RNA Pol II and TOUGH (TGH), suggesting that MTA acts at early stages of miRNA biogenesis. Lack of m^{6}A leads to the stem–loop region of pri-miRNAs becoming less structured, which negatively impacts the binding of Hyponastic Leaves 1 (HYL1) to these precursors. Together, these results suggest that MTA affects Microprocessor assembly via its influence on secondary structure of methylated miRNA precursors, as well as direct interactions between MTA and a miRNA biogenesis protein TGH. Thus, the lack of m^{6}A methylation in pri-miRNAs in the *mta* mutant plants results in the inefficient recruitment of Microprocessor components to plant pri-miRNAs, resulting in their less-efficient processing, and ultimately leading to the decrease in miRNA production. We also suggest that the impaired auxin response in plants with MTA deficiency is caused, at least partly, by decreased miR393b levels in the *mta* mutant plants.

Results

Lack of m^{6}A Results in Impaired miRNA Biogenesis. In order to assess possible effects of m^{6}A on miRNA biogenesis, we performed small RNA (sRNA) sequencing on rosette leaves from 4-wk-old *Arabidopsis* plants of both WT Col-0 and a mutant line with severely reduced m^{6}A levels (*mta* mutant). More specifically, the *mta* mutant line we used contains MTA cDNA under the ABI3 promoter in a homozygous MTA T-DNA insertion mutant background (*mta ABI3:MTA*). The ABI3 promoter drives strong embryo expression of MTA, enabling the plant embryo lethality to be bypassed. However, this promoter drives a very low level of expression postgermination, giving rise to plants with 80 to 90% less m^{6}A modification compared to their WT counterparts (26). Our sequencing data showed a decrease in the overall abundance of mature miRNAs in *mta* mutant as compared to WT plants (*SI Appendix*, Fig. S1). Specifically, we identified 60 differentially expressed miRNAs that had high confidence scores (probability ≥ 0.9 or false-discovery rate ≤ 0.1), and 51 of these 60 miRNAs were found to be down-regulated, while only 9 miRNAs were up-regulated (Fig. 1*A* and *SI Appendix*, Table S1). This down-regulation of miRNAs in *mta* plants was confirmed by quantitative real-time PCR (RT-qPCR) for six arbitrarily selected miRNAs (miR159b, miR169a, miR319b, miR396b, mir399a, and miR850) (Fig. 1*B*).

Next, we went on to investigate the levels of primary miRNAs (pri-miRNAs) in the low methylation plants (*mta* mutants) by using the mirEX^2 platform (www.combio.pl/mirex2) developed by our group (30, 31). This platform utilizes a repository of 298 primer pairs, specifically for *Arabidopsis* pri-miRNA quantification by RT-qPCR. Of the 298 pri-miRNAs tested, 68 pri-miRNAs were at undetectable levels in our samples, leaving 230 for further analysis. The results of RT-qPCR revealed that 85 pri-miRNAs had statistically significant ($P \leq 0.05$, $n = 3$) changes in their accumulation (WT vs. *mta*); 56 of these (∼66%) were found to be up-regulated, while 29 were down-regulated (Fig. 1*C* and *SI Appendix*, Table S1). Upon comparison of the RT-qPCR results with sRNA sequencing data, we identified 20 cognate pri-miRNA/miRNA pairs that showed higher accumulation of pri-miRNAs and lower levels of mature miRNAs (Fig. 1*D*). These results point toward an impaired processing of these pri-miRNAs in the absence of MTA.

***Arabidopsis* pri-miRNAs Are m^{6}A-Methylated by MTA.** The general trend, showing an accumulation of pri-miRNAs and decreased levels of miRNAs in the conditions of reduced m^{6}A methylation, raised the possibility that the presence of m^{6}A is necessary for proper processing of some pri-miRNAs. Therefore, we tested the methylation status of the pri-miRNAs using m^{6}A-RNA immunoprecipitation followed by sequencing (m^{6}A-IP Seq). This method is not an equivalent of the commonly used MeRIPSeq (32), as we avoided the fragmentation of polyA RNA. We validated this protocol using spiked-in methylated and nonmethylated controls (*SI Appendix*, Fig. S2). We further tested the robustness of our data by comparing them to previously published data by Shen et al. (19) and Anderson et al. (33). In our dataset, we were able to identify 14,870 genes whose transcripts (15,562) are depleted in the *mta* mutant, indicating that these gene transcripts are methylated. Upon comparison of our data to the published datasets, we found an overlap of 2,868 (80%) and 3,100 genes (65%) between our data and data from Shen et al. (19) and Anderson et al. (33), respectively; 930 genes were common among all three datasets. A Venn diagram showing these overlaps is presented in *SI Appendix*, Fig. S3.

miRNAs can be encoded within intergenic regions as independent transcriptional units or can be embedded within protein-coding genes sharing transcriptional units with their host protein genes (34). For our analysis from the m^{6}A-IP Seq data we selected transcripts of only those miRNA genes that are independent transcriptional units. Using this approach, we identified transcripts of 11 *MIR* genes that were enriched more than 1.5-fold in WT vs. *mta*, indicating that they are m^{6}A-methylated in WT plants (hence can be immunoprecipitated with m^{6}A antibody), and lack this methylation in the absence of MTA (Fig. 2*A* and *SI Appendix*, Fig. S4). All of the identified pri-miRNAs that passed the enrichment threshold were either absent or had significantly reduced abundance in the *mta* IP sample relative to WT IP.

As an orthogonal approach to verify that these pri-miRNAs were bona fide targets for MTA directed methylation, we carried out RNA IP (RIP) using an anti-GFP antibody and the GFP-tagged MTA (35S:*MTA*-GFP) plant line. As a control, the plants expressing only GFP in the WT Col-0 background were used.

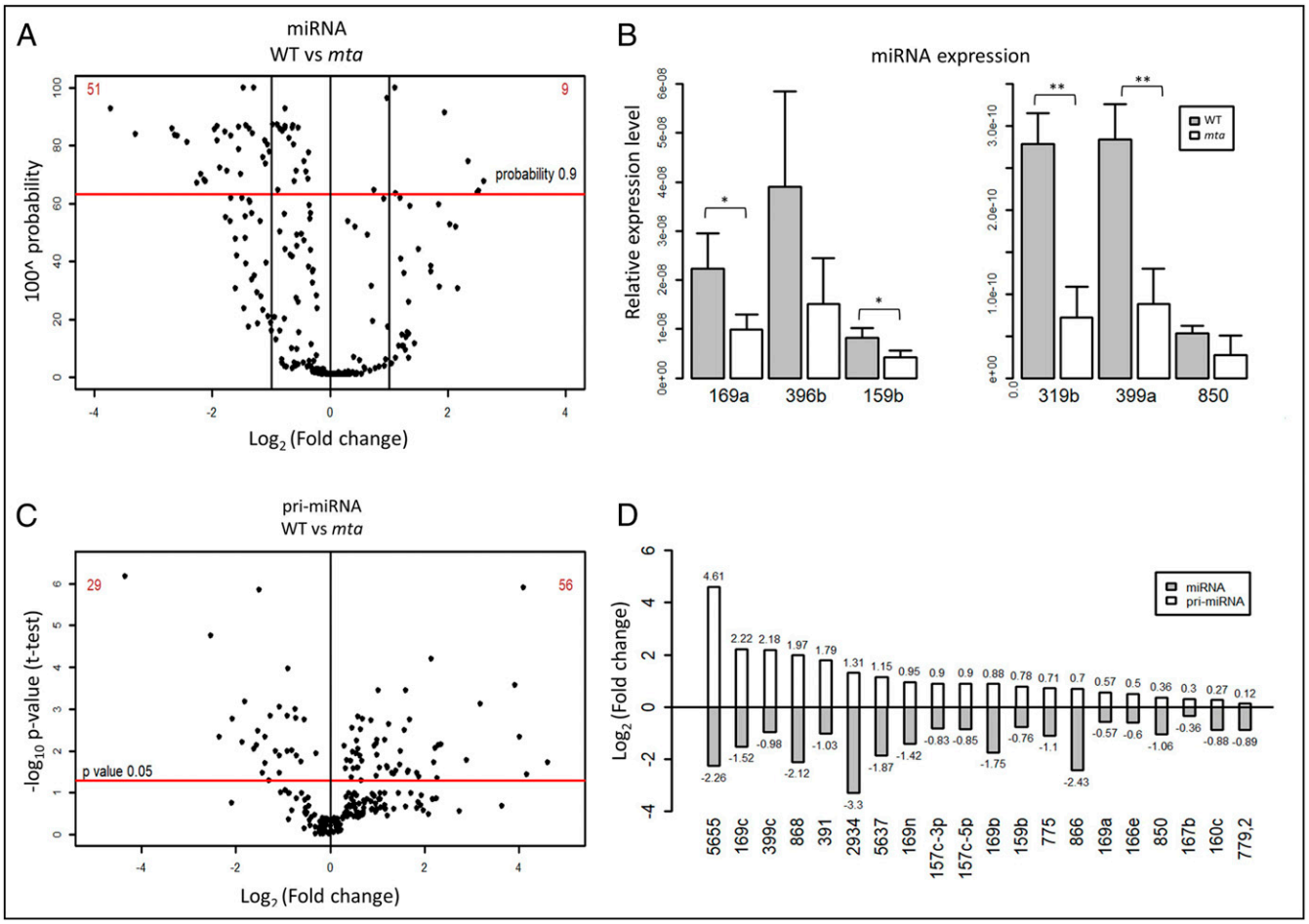

Fig. 1. miRNA biogenesis is impaired in *mta* mutant plants. (*A*) sRNA sequencing analysis of miRNAs in *mta* and WT plants. Each black dot represents one miRNA. The red horizontal bar represents the threshold (probability 0.9). (*B*) Relative abundance (as determined by TaqMan RT-qPCR) of miRNAs identified with altered abundance in WT vs. the *mta* mutant monitored by sRNA sequencing. $*P < 0.05$, $**P < 0.005$, and error bars represent SD ($n = 3$). (*C*) Levels of 230 pri-miRNAs as determined by RT-qPCR with separation of statistically significant pri-miRNAs (above the red horizontal bar). Each dot represents one pri-miRNA and the red horizontal bar represents *P*-value threshold (*P* value 0.05). (*D*) A set of cognate pairs of pri-miRNAs/miRNAs (selected from *A* and *B*) where pri-miRNA levels are up-regulated, while the levels of their cognate miRNA are down-regulated.

RIP was performed on the nuclear fraction and followed by RT-qPCR on oligo(dT) primed cDNA. Eighteen pri-miRNAs (10 from our m^{6}A-IP Seq data and 8 randomly chosen) were selected for verification by RT-qPCR, and of these all but 4 showed a statistically significant enrichment ($P < 0.05$) in the MTA–GFP sample when compared to the GFP control (Fig. 2*B* and *SI Appendix*, Fig. S5). This indicates that pri-miRNAs are frequently bound by MTA. Taken together, these data suggest that MTA binds and methylates at least a set of pri-miRNAs, and that this binding promotes their processing to mature miRNAs.

Lack of m^{6}A Affects Stem–Loop Structure of pri-miRNAs and Their Ability to Bind HYL1. The effect of m^{6}A on secondary structure of RNA has been well documented. Such alterations in RNA structure induced by m^{6}A are known as "m^{6}A switches" (35–37). These m^{6}A switches influence the ability of RNA-binding proteins to recognize the RNA molecules, which further determines the substrate RNA fate. We used protein interaction profile sequencing (PIP-seq) in order to determine whether such structural changes could be observed in miRNA precursors and hence influence miRNA biogenesis. Using this approach, double-stranded RNAs and single-stranded RNAs can be detected after single- and double-stranded specific RNase treatment, respectively (38–40), and thus we were able to identify and distinguish between the structured and unstructured regions of the miRNA precursors. We noticed that the nucleotide accessibility for double- or single-stranded RNase(s) is altered in *mta* mutants. Our data show a significant reduction in the level of pri-miRNA stem–loop structure in the *mta* mutant as compared to WT plants (Fig. 3*A*, two box plots on the left). We observed even stronger differences when we focused only on those pri-miRNAs that we identified as m^{6}A-methylated (Fig. 3*A*, two box plots on the right). By constraining a folding algorithm with PIP-seq–derived structure scores, we obtained 2D structural models for a few examples among the m^{6}A-methylated pri-miRNAs (models for pri-miR160a, pri-miR163a, pri-miR166a, and pri-miR830 are presented in *SI Appendix*, Fig. S6). Presented models represent the most frequently interrogated structural conformation among the potentially multiple existing folding patterns for each RNA. These data-based structural models suggest that the pri-miRNA regions containing the miRNA/miRNA* stem regions tend to be in an unpaired conformation in the absence of the m^{6}A mark (*mta* mutants) as compared to the methylated pri-miRNAs (WT plants) (*SI Appendix*, Fig. S6).

In light of these data, we reasoned that these changes in structure could in principle influence the binding of HYL1 to these precursors. HYL1 is a double-stranded RNA binding

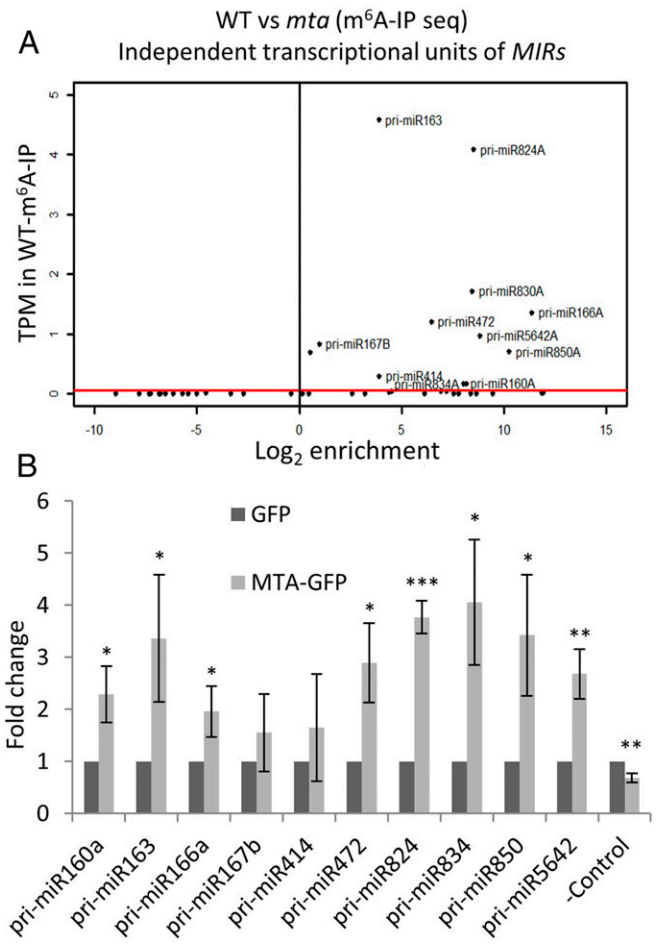

Fig. 2. At least a set of pri-miRNAs are m^{6}A-methylated by MTA. (*A*) *MIR* gene transcript identified by m^{6}A-IP Seq. The red bar represents the threshold of transcripts per million (TPM) > 0.05. (*B*) Levels of pri-miRNAs in MTA-GFP samples after GFP trap-based RIP followed by RT-qPCR are presented as fold-changes as compared to the GFP control. *P < 0.05, **P< 0.005, ***P < 0.001. Error bars represent SD of three biological replicates. –Control = AT2G40000 gene.

protein and is an important player in miRNA biogenesis (41, 42). Hence, we studied the binding of HYL1 to pri-miRNAs in WT and *mta* mutant plants using RIP (HYL1-RIP) followed by RT-qPCR. We found that 7 of the 10 pri-miRNAs tested were significantly less abundant in HYL1-IP samples from the *mta* mutants as compared to WT (Fig. 3*B*). A decrease in the binding efficiency of HYL1 that is a double-stranded RNA binding protein, to pri-miRNAs in the *mta* mutant is an additional indication that a double-stranded conformation of miRNA/miRNA* containing stem–loop regions of pri-miRNAs are formed less frequently in low methylation (*mta*) than in WT plants.

MTA Interacts with RNA Pol II In Situ. The strong tendency toward accumulation of pri-miRNAs and low abundance of miRNAs in *mta* mutants is reminiscent of various *Arabidopsis* mutants of genes encoding the proteins that participate in miRNA biogenesis, like Dicer-like 1 (DCL1), HYL1 (42–44), Serrate (SE) (45), and TGH (46). These proteins are involved in early stages of miRNA biogenesis and are needed for efficient processing of pri-miRNAs to miRNAs. These observations led us to suggest that MTA might act at early stages of miRNA biogenesis, probably cotranscriptionally. The deposition of m^{6}A is usually assumed to be cotranscriptional; this assumption is supported by the fact that m^{6}A can influence other processing events, such as selection of polyadenylation sites or pre-mRNA splicing, which are themselves cotranscriptional (47–49). However, a direct association between METTL3 and RNA Pol II has only been shown in mammalian cells when the rate of transcription was artificially slowed down (50). We confirmed colocalization of MTA and RNA Pol II in *Arabidopsis* using immunolocalization (*SI Appendix*, Fig. S7). Furthermore, we used the proximity ligation assay (PLA) to confirm in vivo interactions of MTA with RNA Pol II in plants under physiological conditions. Our results show direct interactions between MTA–GFP and RNA Pol II in cell nuclei with MTA–GFP expression but not in the GFP control (Fig. 4). These results were obtained for RNA Pol II phosphorylated at both Serine 5 and Serine 2. Thus, we show that MTA is associated with the RNA Pol II from an early stage of transcription and likely methylates pri-miRNAs (among other RNA Pol II transcripts) cotranscriptionally.

MTA Acts at Early Stages of miRNA Biogenesis. While MTA interacting with RNA Pol II is an indication of it methylating RNA Pol II transcripts cotranscriptionally in general, we investigated whether specific proteins involved in miRNA biogenesis could interact with MTA. To address this possibility, we performed a screen on possible MTA interactors involved in early steps of miRNA biogenesis, like HYL1, Cap binding protein 20 (CBP20), SE, TGH, and Dawdle (DDL1), using a microscopic approach. We performed FRET analyzed by fluorescence lifetime imaging microscopy (FLIM). As FRET can occur only when two proteins are within nanometers of each other, FRET–FLIM helps to quantify direct protein–protein interactions. This FRET–FLIM analysis confirmed the close association and interactions of MTA and TGH (Fig. 5). No such interactions could be seen in the case of any other tested proteins (*SI Appendix*, Fig. S8). Thus, we identified the miRNA biogenesis factor TGH as an MTA partner.

Lack of m^{6}A/MTA Impairs Microprocessor Complex Assembly. Having identified TGH as an interactor of MTA, we focused on the m^{6}A methylation status of pri-miRNAs in the *tgh* mutant. m^{6}A-IP followed by RT-qPCR revealed that except for two pri-miRNAs, there is no overall significant reduction of m^{6}A methylation in pri-miRNAs in the *tgh* mutant (*SI Appendix*, Fig. S9). This result indicates that TGH is not required for m^{6}A methylation, and MTA acts upstream of TGH in miRNA biogenesis.

It is known that during miRNA biogenesis, TGH facilitates DCL1 action and pri-miRNA processing via promoting the pri-miRNA–HYL1 interaction (46). We then tested whether a lack of MTA, and hence loss of the MTA–TGH interaction, could also affect Microprocessor assembly. Using coimmunolocalization, we determined that in the *tgh* mutant DCL1 colocalization with RNA Pol II (phosphorylated at Serine 2) is significantly reduced. We found a similar level of reduction in DCL1 colocalization with RNA Pol II in the *mta* mutant (Fig. 6 *A* and *B*). Similarly, HYL1 colocalization with RNA Pol II is also reduced in *mta* mutant plants similar to the *tgh* mutant (Fig. 6 *C* and *D*). The observation that the lack of either TGH or MTA hampers colocalization of RNA Pol II with DCL1 and HYL1 suggests that MTA facilitates Microprocessor assembly either by attracting TGH via direct MTA–TGH interaction or with help of an additional m^{6}A reader protein (unknown so far).

MTA Regulates the Level of miR393b which Is Involved in Auxin Response. Auxin response defects have been reported for hypomorphic mutants of the known plant m^{6}A methyltransferase complex (20). We found this to be the case for the auxin-responsive *DR5pro:GUS* reporter construct when introduced into both WT and the *mta* mutant background. Upon induction of 14-d-old seedlings with 2,4-dichlorophenoxyacetic acid (2,4-D), the *mta* plants showed much less GUS expression (Fig. 7*A*).

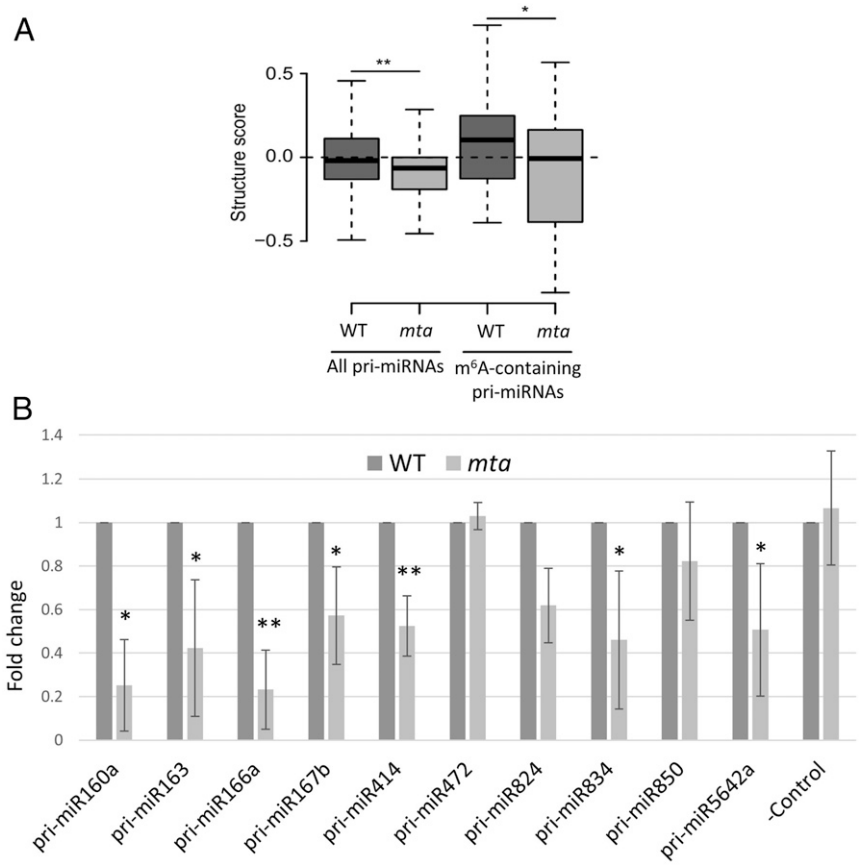

Fig. 3. The structures of miRNA precursors and their binding to HYL1 is altered in absence of m^{6}A. (*A*) Box plots show a decrease in the structure scores of miRNA precursors. All miRNA precursors include 235 precursors whose data are accessible from the PIP-seq analysis (two box plots on the left). m^{6}A-containing precursors refer to the 11 pri-miRNA examples found as m^{6}A-methylated in this study (two box plots on the right). (*B*) Levels of pri-miRNAs in *mta* mutants after HYL1-RIP RT-qPCR are presented as fold-changes as compared to WT control. Error bars represent SD of three biological replicates. *$P < 0.05$, **$P < 0.005$. –Control = *WUSCHEL (WUS)* gene (AT2G17950).

miR393b has been described to be involved in auxin response regulation, and in mutants lacking miR393b, auxin signaling is reduced (51). In our sRNA sequencing data, we found that miR393b is down-regulated in *mta* mutants, although we could not detect its precursor in our m^{6}A-IP Seq. However, because of its recognized importance in regulating auxin responses, we further investigated the requirement of m^{6}A for miR393b accumulation. We confirmed that pri-miR393b is m^{6}A-methylated using m^{6}A-IP followed by RT-qPCR. IP of RNA bound to MTA also confirmed MTA binding to pri-miR393b (Fig. 7*B*). Interestingly, our PIP-seq analysis revealed that pri-miR393b is less structured in *mta* than in WT plants. Moreover, the 2D model of this precursor revealed that its stem–loop region that contains mature miR393b sequence is formed more efficiently when pri-miR393b contains m^{6}A (WT) in comparison to unmethylated precursors (*mta* mutant), similar to the other miRNAs showing underaccumulation in *mta* mutant plants in comparison to WT (*SI Appendix*, Fig. S10).

To further demonstrate that the low expression level of miR393b is in fact caused by the lack of MTA, we designed a transient expression assay in *Nicotiana benthamiana*. We used constructs designed to express pri-miR393b, MTA, or a catalytically inactive version of MTA, ΔMTA (D482A). ΔMTA was prepared by primer-induced point mutation resulting in the following change: Aspartic acid at position 482 to alanine (D482A) at the catalytic DPPW motif (52), making the protein catalytically inactive. These were introduced individually or in combination into *Nicotiana* leaves by agroinfiltration. We then assessed mature miR393b levels by Northern blot and found that the pri-miRNA393b transgene produces ∼2.3 times more miR393b when it is coexpressed with MTA, while this effect was abolished to a large extent when MTA was replaced by its catalytically inactive version (ΔMTA) (Fig. 7*C*). Thus, we show that the reduced auxin response in *mta* mutant plants is partially caused by the regulatory defects of miR393b biogenesis due to the lack of MTA activity.

Discussion

Here, we provide evidence that, in addition to influencing mRNA metabolism, m^{6}A methylation is present in pri-miRNAs and affects miRNA biogenesis in *A. thaliana.* We show that the lower level of MTA (and hence m^{6}A) leads to a reduction of miRNA levels in the case of at least 25% of miRNAs, whereas pri-miRNAs tend to overaccumulate in the mutant plants. This anticorrelation of pri-miRNAs with miRNA levels is reminiscent of observations from the *Arabidopsis* lines carrying mutations in genes encoding proteins involved in early stages of miRNA biogenesis: For example, *hyl1* (42–44) and *se* (45). In contrast, mutants of HEN1 [a protein that is involved in methylation of miRNA/miRNA* duplexes at the 3′ ends (53), thus acting at the later step of miRNA biogenesis] do not show accumulation of pri-miRNAs, while down-regulation of miRNAs is observed in *hen1* mutant plants (54). This suggests that MTA regulates miRNA production at early stages of their biogenesis.

Since MTA is a known mRNA methyltransferase and m^{6}A is abundant in mRNA, we considered the possibility that the

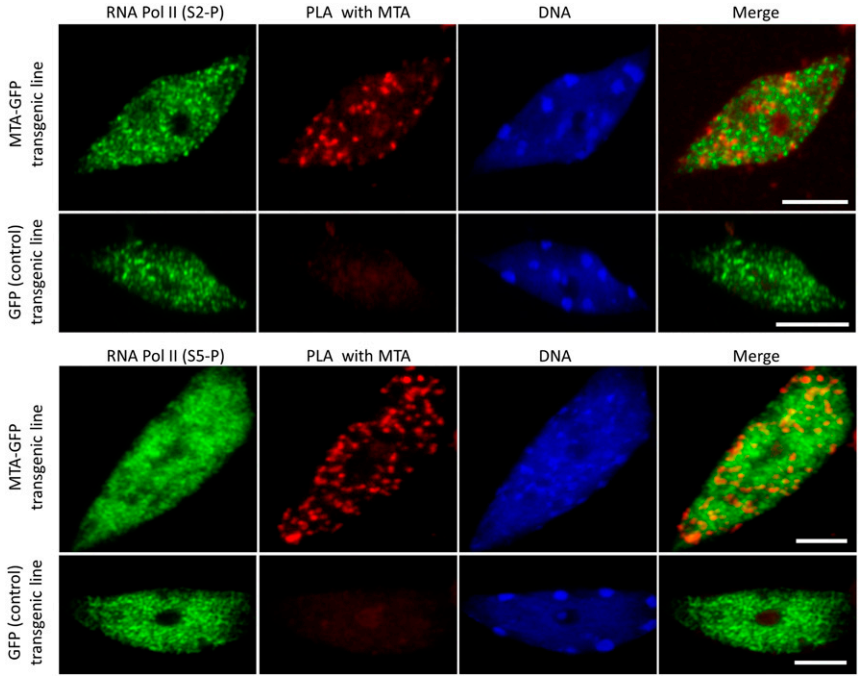

Fig. 4. PLA shows the interaction between MTA and RNA Pol II phosphorylated at Serine 2 and Serine 5. Positive PLA signals (red spots in the second column) can be seen only in cells containing the MTA–GFP transgene, but not in control cells expressing GFP alone. RNA Pol II is represented in green. DNA is stained with HOECHST (blue). (Scale bars, 5 μm.)

observed effects were indirect and can be a result of altered metabolism of other miRNA biogenesis proteins. We used two different and independent approaches to exclude this possibility. MTA–GFP-mediated RNA IP and m^6A-IP experiments revealed that for at least a group of miRNAs, this effect is direct and is a result of MTA binding to pri-miRNAs and introducing m^6A marks. Additionally, structural changes in the pri-miRNAs characterized by the loss of secondary structure and increase in single-stranded regions in the *mta* mutant background, specifically in the stem–loop regions of these miRNA precursors, also indicate the importance of m^6A in miRNA biogenesis in plants. These structural analyses go in line with less efficient binding of HYL1, a double-stranded RNA binding protein, to unmethylated pri-miRNAs in the *mta* mutant.

Our studies also revealed that MTA can directly interact with TGH, a protein involved in early stages of miRNA biogenesis. As many other miRNA biogenesis mutants, *tgh* shows a decrease in accumulation of miRNAs and overaccumulation of many pri-miRNAs. Moreover, TGH has been described as a factor important for the recruitment of HYL1 to pri-miRNAs (46). Thus, MTA can influence miRNA biogenesis in two different ways: 1) by m^6A methylation of miRNA precursors, and/or 2) by direct interactions with TGH. We show that the m^6A marks introduced by MTA stabilize the secondary structure of the stem loop regions of pri-miRNAs, likely stimulating their recognition by HYL1, and afterward by the endonuclease DCL1 as well as the rest of the components of the Microprocessor complex. However, MTA may also stimulate Microprocessor assembly by its direct interactions with TGH, which in turn interacts with HYL1 and stimulates/stabilizes HYL1 binding to double-stranded regions of pri-miRNAs. Upon comparison of our results to the previously published data regarding miRNA levels in the *tgh* mutant, we found a 45% overlap within down-regulated miRNAs in both *tgh* and *mta* mutants, despite these two datasets originating from two different tissues (46) (*SI Appendix*, Fig. S11). These 23 miRNAs that are down-regulated in both *mta* and *tgh* mutants could be regulated by the direct MTA–TGH interactions. However, the mechanism of this MTA–TGH interaction-related alteration of miRNA biogenesis requires further studies.

Here, we also provide evidence that MTA interacts with RNA Pol II phosphorylated at both Serine 5 and Serine 2. This shows

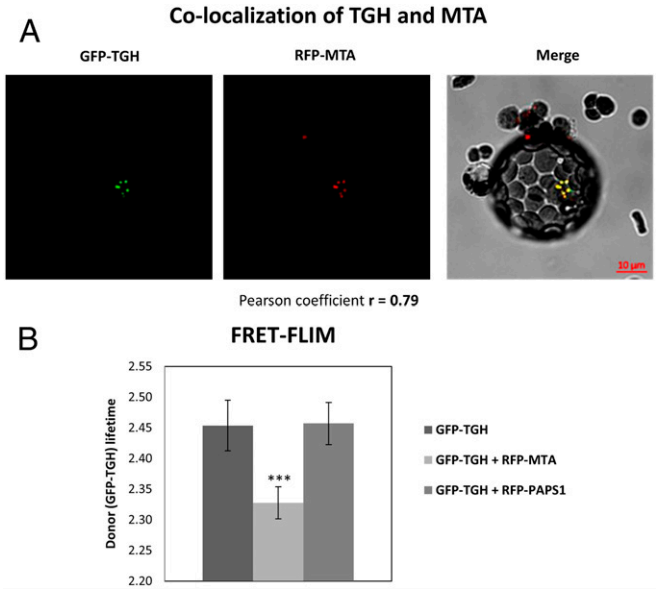

Fig. 5. MTA interacts with the miRNA biogenesis related protein TGH. (*A*) *Arabidopsis* WT protoplasts cotransfected with GFP–TGH and RFP-MTA (*Left* and *Center*), showing colocalization of both proteins in the nucleus. (*Right*) A merged image. (*B*) FRET–-FLIM analysis in *Arabidopsis* protoplasts cotransfected with GFP–TGH and RFP–MTA, or GFP–TGH and RFP–PAPS1 [PAPS1 stands for Poly(A) Polymerase 1, used here as a control protein]. Reduction in a donor lifetime (GFP–TGH) was seen with RFP–MTA but not with the negative control (RFP–PAPS1); $***P < 0.001$, $n = 9$.

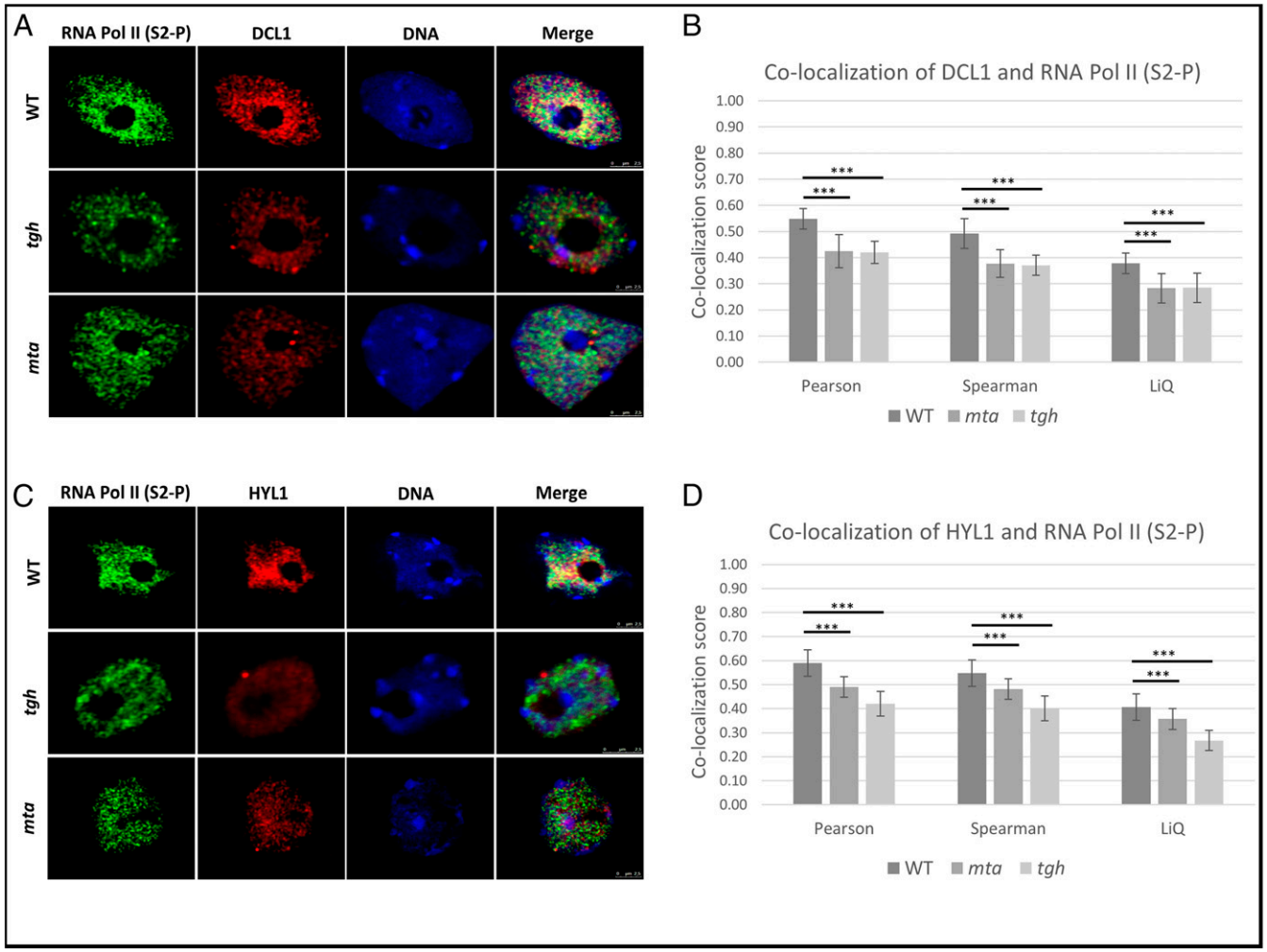

Fig. 6. Microprocessor assembly is impaired in both *mta* and *tgh* mutants. (*A*) Localization of RNA Pol II (green), DCL1 (red), and DNA (blue) in the nuclei of WT plants as well as *mta* and *tgh* mutants. (*B*) Colocalization scores of DCL1 and RNA Pol II are significantly lower in *mta* and *tgh* mutants as calculated using three different approaches (Pearson, Spearman, and LiQ). (*C*) Localization of RNA Pol II (green), HYL1 (red), and DNA (blue) in the nuclei of WT plants as well as *mta* and *tgh* mutants. The merge column shows all three channels. (*D*) Colocalization scores of HYL1 with RNA Pol II are significantly lower in *mta* and *tgh* mutants as calculated by three different approaches (Pearson, Spearman, and LiQ). ***$P < 0.001$, $n = 50$.

that MTA is associated with the RNA Pol II from the initiation of transcription and is present during the elongation step, modifying growing transcripts (see ref. 55 for review). In both *mta* and *tgh* mutants, colocalization of HYL1 and DCL1 with the elongation form of RNA Pol II (phosphorylated at Serine 2) is impaired, suggesting that both MTA/m^{6}A as well as TGH contribute to cotranscriptional assembly of the Microprocessor.

In addition to the miRNAs that show decreased levels in the absence of m^{6}A methylation, we also noticed nine miRNA species whose levels were up-regulated in *mta* hypomorphic plants. Interestingly, four precursors of these miRNAs adopt more structured conformations in low methylation plants (*mta* mutant) than in plants with the regular level of MTA (WT) (*SI Appendix*, Fig. S12). This may suggest that in some rare cases the absence of MTA or m^{6}A methylation can have a positive effect on the proper conformation of pri-miRNAs. However, none of these precursors were shown to be m^{6}A methylated, as demonstrated by our m^{6}A-IP Seq. Moreover, they were also not found in any of the published lists of m^{6}A-methylated *Arabidopsis* transcripts (19, 33). Thus, it is unlikely that the increased levels of the nine miRNAs in the *mta* mutant is connected to their pri-miRNA's methylation or recognition by MTA, but rather it is an indirect effect of the lack of MTA activity, most probably via 1) pri-miRNA alternative splicing or polyA site selection or 2) up-regulation of transcription factors (either directly regulated by m^{6}A mRNA methylation or regulated by miRNAs that are down-regulated in the *mta* mutant) stimulating their transcription. To answer which of these mechanisms are involved in the up-regulation of some miRNAs in *mta* plants, additional studies are required.

We also noticed that 29 pri-miRNAs were less abundant in *mta* in comparison to WT plants. Of these 29 pri-miRNAs, only 1 (pri-miR472) has been shown to be recognized and bound by MTA, and is m^{6}A-modified. The additional 28 pri-miRNAs are most likely not m^{6}A-methylated, so their lower accumulation cannot be directly explained by the presence of m^{6}A marks, but rather by indirect effects. We show that HYL1 binds to pri-miR472 independently whether it is methylated (WT) or not (*mta* plants), and the level of mature miR472 in the *mta* mutant is similar to that observed in WT plants. This may suggest that the lack of MTA does not influence Microprocessor assembly on miR472 precursors. However, loss of MTA, hence m^{6}A methylation of pri-miR472, affects the level of pri-miR472, which is decreased in low m^{6}A methylation plants. It is worth noting that

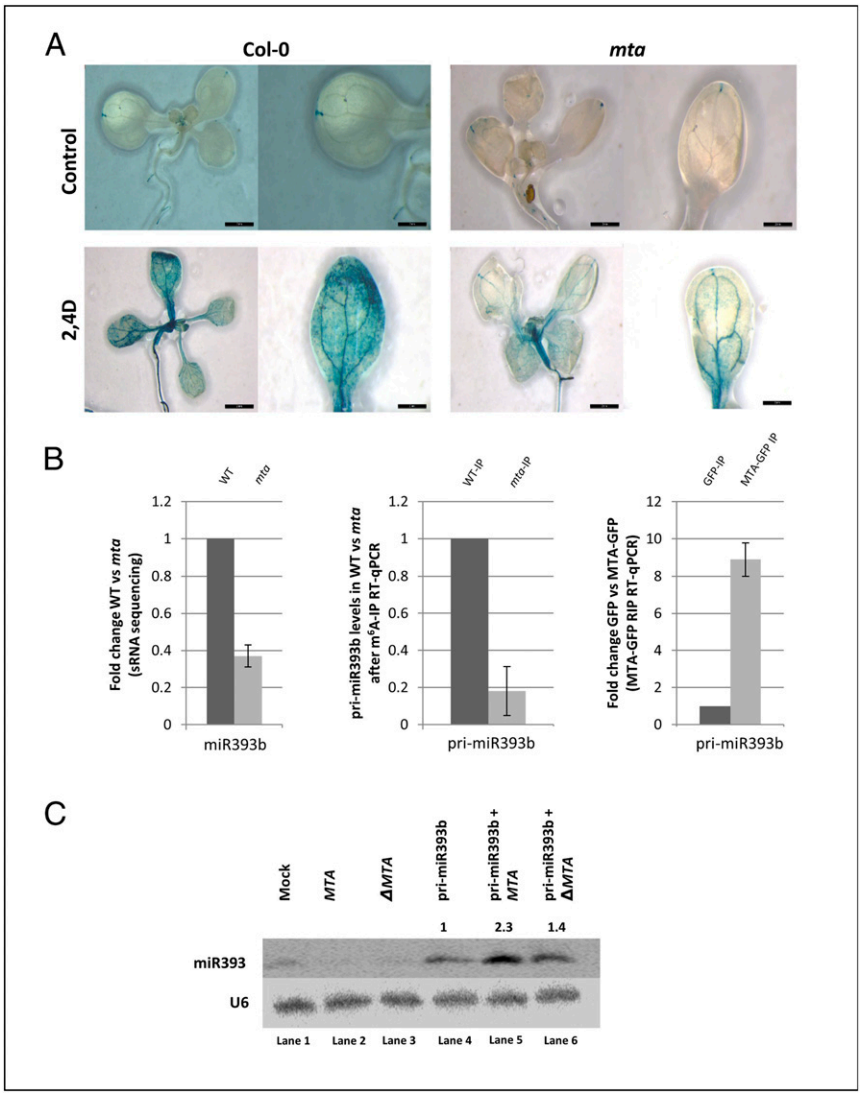

Fig. 7. Auxin insensitivity in the *mta* mutant correlates with loss of methylation of pri-miR393b and the low level of mature miR393b. (*A*) Expression of auxin-responsive reporter *DR5pro:GUS* construct in the *mta* mutant background is reduced upon treatment with auxin (2,4-D). Strong inhibition of auxin response after induction is observed in the *mta* mutant. (Scale bars, 2 mm.) (*B*) The miR393b level is down-regulated in the *mta* mutant (sRNA sequencing data) as compared to WT plants (*Left*, $n = 3$), pri-miR393b carries m^{6}A mark (m^{6}A-IP followed by RT-qPCR, *Center*, $n = 3$), and pri-miR393b is bound by MTA (MTA-GFP RIP, *Right*, $n = 3$). Graphs represent fold-change values between WT and *mta* mutant plants (*Left* and *Center*) and GFP and MTA-GFP plants (*Right*). (*C*) *N. benthamiana* leaves were agroinfiltrated with one of following constructs: MTA, catalytically inactive MTA (ΔMTA), and pri-miR393b (lanes 2, 3, and 4, respectively) or with a combination of two constructs [encoding pri-miR393b + the construct encoding MTA (lane 5) or pri-miR393b + ΔMTA (lane 6)]. The levels of miR393b were monitored for each experimental variant using Northern blotting. Mock represents transfection with no plasmid control, and U6 serves as a loading control. Numbers above the last three lanes represent relative amounts of miR393b in the presence of MTA (2.3, penultimate lane) or ΔMTA (1.4, last lane) as compared to the expression of pri-miR393b alone (1, lane 4).

the *Arabidopsis MIR* gene encoding miR472 is very long (~5 kbp) and contains four exons (31). Its transcription ends at several alternative polyadenylation sites and the transcripts undergo alternative splicing. Thus, it is also possible that m^{6}A methylation of pri-miR472 changes maturation of *MIR472* primary transcripts toward variants that are efficiently processed into mature miR472. This would explain the lower level of pri-miR472 and the constant level of miR472 in *mta* plants in comparison to WT. However, additional studies are needed to verify this interesting scenario.

As already mentioned above, while analyzing effects of m^{6}A methylation on miRNA biogenesis, one should be aware that miRNA biogenesis is affected by a variety of processes like splicing, alternative polyadenylation, degradation, and so forth (56–60). The changes in structure caused by m^{6}A can influence all of these processes by altering binding of proteins to *MIR* primary transcripts. The possible role of an m^{6}A reader protein in the processing of pri-miRNAs should also not be overlooked. The overall expanse of m^{6}A presence and the magnitude of its possible effects on miRNA biogenesis needs to be investigated and this work opens a new fascinating avenue for such future studies.

Interestingly, the reduced auxin responsiveness of m^{6}A writer mutant plants can be partially explained by the altered miR393b level. We show that pri-miR393b is m^{6}A-methylated by MTA, and the level of miR393b is lower in the *mta* mutant in comparison to WT plants. miR393b is involved in homeostasis of *AUX/IAA* genes the expression of which is regulated by a complex feedback loop that involves regulation of these genes by the proteins they encode (51, 61, 62). miR393b has been shown to accumulate in leaves and is induced in response to auxin (52). We have found that expression of the auxin responsive *DR5pro:GUS*

reporter is reduced in *miR393b* mutant plants (51) and a similar reduction is seen with the same reporter in the *mta* background. Thus, the altered miR393b biogenesis in the plants with the low level of m^6A methylation of pri-miRNAs likely contributes to the reduced auxin response in the m^6A writer mutant, linking this modification with miRNA biogenesis and, as a physiological effect, with one of the most crucial hormone response pathways.

Based on our results, we propose a model showing the involvement of MTA/m^6A in miRNA biogenesis in plants. m^6A methylation of pri-miRNAs influences miRNA precursor secondary structure that in consequence stimulates the recognition of pri-miRNAs by HYL1. The direct interactions between MTA and the TGH protein and recognition of m^6A marks by an unknown m^6A reader that may also interact with TGH may also be involved in the HYL1 recruitment to the methylated miRNA precursor. This is strongly supported by the previously described involvement of TGH in the HYL1 recruitment to pri-miRNAs (46). Thus, the recognition of pri-miRNAs by HYL1, and in consequence assembly of the whole active Microprocessor, is controlled by pri-mRNA m^6A methylation, which induces the proper secondary structure of the precursor as well as a specific MTA–TGH interaction that both support efficient assembly of the plant miRNA biogenesis machinery (Fig. 8).

Materials and Methods

Plant Material. *A. thaliana* WT Col-0, *mta* mutants (26), MTA-GFP (*p35S:MTA-GFP*), and GFP plants were sown on Jiffy pots and stratified for 2 d in dark at 4 °C. Thereafter, the plants were grown in plant growth chambers at 22 °C with 16-h light and 8-h dark cycles (70% humidity, 150- to 200-μmol m^{-2} s^{-1} photon flux density). Rosette leaves from 4-wk-old plants were harvested, immediately flash-frozen in liquid nitrogen, and used or stored at −80 °C until further use.

sRNA Sequencing and Analysis. sRNA fraction from 4-wk-old *A. thaliana* WT Col-0 and *mta* mutant plants was used to prepare libraries that were sequenced at Fasteris on the HiSeq 4000 platform. A detailed description of the library preparation and data analysis can be found in *SI Appendix, Supplementary Materials and Methods*.

m^6A-RNA IP of pri-miRNAs and Sequencing. PolyA enriched RNA from 4-wk-old *A. thaliana* WT Col-0 and *mta* mutant plants was used to perform m6A IP. Libraries were prepared from RNA before IP (input) and after (IP). A detailed description of the library preparation and data analysis can be found in *SI Appendix, Supplementary Materials and Methods*.

Data Submission and Availability. The data obtained in this study (sRNA and m^6A-IP Seq) has been deposited under the National Center for Biotechnology Information (NCBI) Gene Expression Omnibus (GEO) accession no. GSE122528. The PIP-seq data used for the secondary structure analysis of miRNA transcripts can be found under NCBI GEO accession no. GSE108852.

RIP. Transgenic *Arabidopsis* line *p35S:MTA-GFP* and *mta* mutants were grown along with the GFP and WT *Arabidopsis* lines. RIP was performed as described by Raczynska et al. (63). A detailed protocol for RIP and data analysis can be found in *SI Appendix, Supplementary Materials and Methods*.

PIP-Seq Analysis to Access RNA Structure Scores of miRNA Processors. A total of two biological replicates of PIP-seq, including single-stranded RNA-seq and double-stranded RNA-seq libraries, for leaves five to nine from 4-wk-old WT and *mta* mutant plants were constructed as previously described (37, 39). The raw data has been deposited under the GEO accession no. GSE108852. Refer to *SI Appendix, Supplementary Materials and Methods* for the detailed protocol and data analysis pipeline.

Immunolocalization. The immunolabeling experiments using the Duolink PLA fluorescence protocol were performed on isolated nuclei of 4-wk-old *A. thaliana* leaves (WT, plants with MTA-GFP expression or GFP expression, *mta* and *tgh* mutants). Before isolation, the leaves were fixed in 4% paraformaldehyde in PBS, pH 7.2, for 1 h, washed three times in PBS at room temperature, and then the nuclei isolation protocol according to the method of Pontvianne et al. (64) was followed.

Double Immunodetection of RNA Pol II with MTA, DCL1, and HYL1. A detailed description of double-immunodetection protocol and the accompanying statistical analysis can be found in *SI Appendix, Supplementary Materials and Methods*.

PLA. PLA was performed on isolated nuclei from leaves of MTA-GFP and GFP (control) lines. In situ PLA detection was carried out using the appropriate Duolink in situ Orange Kit Goat/Rabbit (Sigma-Aldrich) according to the protocol of the manufacturer. A detailed protocol for PLA can be found in *SI Appendix, Supplementary Materials and Methods*.

FRET–FLIM. FRET–FLIM was performed using protoplasts were isolated from 3- to 4-wk-old WT *Arabidopsis* leaves using the method described in Knop et al. (65). For the detailed protocol, please refer to *SI Appendix, Supplementary Materials and Methods*.

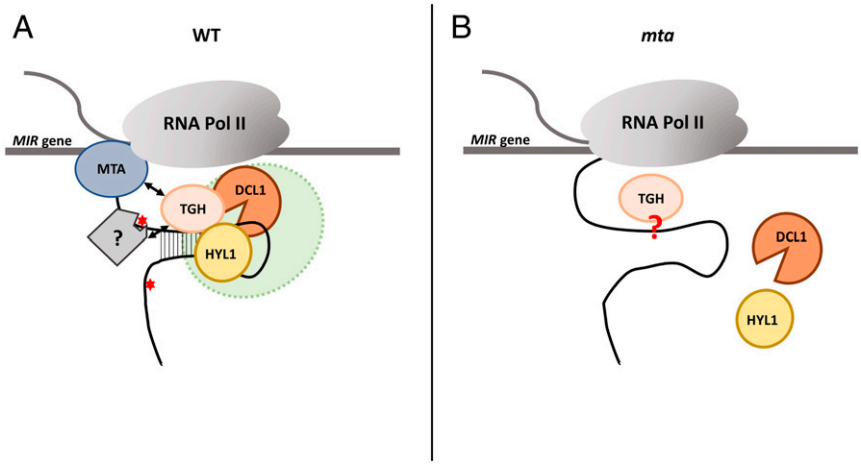

Fig. 8. A schematic representation of the role of m^6A/MTA in miRNA biogenesis in plants. (*A*) In WT plants (*Left*), MTA methylates at least a set of pri-miRNAs which in turn leads to folding the proper secondary structure of a miRNA precursor. MTA and/or a putative reader of the m^6A marks introduced by this enzyme (a gray square marked with "?") facilitate the binding of TGH to the pre-miRNA. The properly folded miRNA precursor is recognized by HYL1. This eventually leads to efficient Microprocessor assembly and miRNA biogenesis at the appropriate level. (*B*) In the *mta* mutant, the lack of MTA, and thus m^6A, leads to the loss of MTA–TGH interactions and inefficient formation of a stem–loop structure in the miRNA precursor, leading to reduced binding of HYL1 that in consequence disrupts Microprocessor assembly, and finally the down-regulation of the mature miRNA level is observed. Whether TGH can bind to the precursor in the *mta* mutant is unknown (marked in the scheme by a red question mark).

GUS Staining for Auxin Response Analyses. Fourteen-day-old seedlings of WT and *mta* mutants with the *DR5pro:GUS* reporter gene construct were incubated in 1/2 MS medium containing 10 μM 2,4-D in ethanol or in ethanol alone as a control for 8 h. After GUS staining the pictures were taken using the Leica M60 stereo microscope.

pri-miR393b, MTA, and ΔMTA Constructs. pri-miR393b (sequence from mirEX[2], www.combio.pl/mirex2) and MTA cDNA (AT4G10760) were amplified and cloned into pENTR/D-TOPO vectors (Thermo Fischer Scientific). ΔMTA was prepared by a primer-induced point mutation resulting in the following change: Aspartic acid at position 482 was changed to alanine (D482A) at the catalytic DPPW motif. For transient expression in *N. benthamiana*, these sequences were then cloned into pMDC32 using the Gateway (Thermo Fisher Scientific) cloning system.

***N. benthamiana* Transient Expression.** pri-miR393b, MTA, and ΔMTA constructs were transformed into *Agrobacterium tumefaciens* (AGL1) using electroporation. After verification of constructs in *Agrobacterium* by sequencing, tobacco leaves were transformed as described by Bielewicz et al. (56). Leaves were transformed either with pri-miR393b, MTA, and ΔMTA alone or in combinations (pri-miR393b + MTA, pri-miR393b + ΔMTA); leaves were harvested after 72 h and RNA isolation (as described above) was followed by Northern blotting.

Northern Blotting. Northern blotting was performed as described in Kruszka et al. (66). Briefly: 30 μg of RNA (per sample) isolated from transfected tobacco leaves was loaded on 8 M denaturing urea polyacrylamide gel (15%) in TBE buffer (0.089 M Tris, 0.089 M boric acid, and 0.002 M EDTA, pH 8.0). RNA was then transferred onto the Amersham Hybond-NX nitrocellulose membrane (GE Healthcare) using a Trans-Blot Electrophoretic Transfer Cell (Bio-Rad) and fixed using CL-1000 UV Crosslinker (UVP). Prehybridization and hybridization were performed in hybridization buffer (3.5% SDS, 0.375 M sodium phosphate dibasic, 0.125 M sodium phosphate monobasic) at 42 °C with DNA oligo probes (Sigma) labeled at their 5′ ends with γ^{32}P ATP (Hartmann Analytic). U6 was used as a loading control. After washing, the blots were exposed for up to 3 d to a phosphorimaging screen (Fujifilm) and the results were visualized with the Fujifilm FLA5100 reader (Fujifilm) and quantified using Multi Gauge V2.2 (Fujifilm).

Data Availability. The data reported in this paper have been deposited in the NCBI GEO database, https://www.ncbi.nlm.nih.gov/geo (accession nos. GSE122528 and GSE108852).

ACKNOWLEDGMENTS. This work was funded by the Polish National Science Centre (Grants UMO-2019/32/T/NZ1/00122, UMO-2017/27/N/NZ1/00202, UMO-2016/23/B/NZ9/00862, UMO-2016/23/D/NZ1/00152, UMO-2013/10/A/NZ1/00557). The authors also received financial support from the Initiative of Excellence–Research University (05/IDUB/2019/94) at Adam Mickiewicz University, Poznan, Poland, and from the Poznan RNA Research Centre. Work in the R.G.F.'s laboratory was supported by the Biotechnology and Biological Sciences Research Council (Grant BB/M008606/1). Work in B.D.G.'s laboratory was supported by the National Science Foundation (Grants MCB-1623887 and IOS-1444490).

1. Y. Yang, P. J. Hsu, Y. S. Chen, Y. G. Yang, Dynamic transcriptomic m^{6}A decoration: Writers, erasers, readers and functions in RNA metabolism. *Cell Res.* **28**, 616–624 (2018).
2. J. A. Bokar, M. E. Shambaugh, D. Polayes, A. G. Matera, F. M. Rottman, Purification and cDNA cloning of the AdoMet-binding subunit of the human mRNA (N6-adenosine)-methyltransferase. *RNA* **3**, 1233–1247 (1997).
3. Y. Pan, P. Ma, Y. Liu, W. Li, Y. Shu, Multiple functions of m^{6}A RNA methylation in cancer. *J. Hematol. Oncol.* **11**, 48 (2018).
4. M. Brocard, A. Ruggieri, N. Locker, m^{6}A RNA methylation, a new hallmark in virus-host interactions. *J. Gen. Virol.* **98**, 2207–2214 (2017).
5. B. Tan, S.-J. Gao, RNA epitranscriptomics: Regulation of infection of RNA and DNA viruses by N^6 -methyladenosine (m^6 A). *Rev. Med. Virol.* **28**, e1983 (2018).
6. J. Liu *et al.*, A METTL3-METTL14 complex mediates mammalian nuclear RNA N6-adenosine methylation. *Nat. Chem. Biol.* **10**, 93–95 (2014).
7. X.-L. Ping *et al.*, Mammalian WTAP is a regulatory subunit of the RNA N6-methyladenosine methyltransferase. *Cell Res.* **24**, 177–189 (2014).
8. S. Schwartz *et al.*, Perturbation of m^{6}A writers reveals two distinct classes of mRNA methylation at internal and 5′ sites. *Cell Rep.* **8**, 284–296 (2014).
9. D. P. Patil *et al.*, m(6)A RNA methylation promotes XIST-mediated transcriptional repression. *Nature* **537**, 369–373 (2016).
10. J. Wen *et al.*, Zc3h13 regulates nuclear RNA m^{6}A methylation and mouse embryonic stem cell self-renewal. *Mol. Cell* **69**, 1028–1038.e6 (2018).
11. P. Knuckles *et al.*, Zc3h13/Flacc is required for adenosine methylation by bridging the mRNA-binding factor Rbm15/Spenito to the m^{6}A machinery component Wtap/Fl(2)d. *Genes Dev.* **32**, 415–429 (2018).
12. C. Xu *et al.*, Structural basis for selective binding of m^{6}A RNA by the YTHDC1 YTH domain. *Nat. Chem. Biol.* **10**, 927–929 (2014).
13. X. Wang *et al.*, N6-methyladenosine modulates messenger RNA translation efficiency. *Cell* **161**, 1388–1399 (2015).
14. H. Du *et al.*, YTHDF2 destabilizes m(6)A-containing RNA through direct recruitment of the CCR4-NOT deadenylase complex. *Nat. Commun.* **7**, 12626 (2016).
15. H. Shi *et al.*, YTHDF3 facilitates translation and decay of N^6-methyladenosine-modified RNA. *Cell Res.* **27**, 315–328 (2017).
16. G. Jia *et al.*, N6-methyladenosine in nuclear RNA is a major substrate of the obesity-associated FTO. *Nat. Chem. Biol.* **7**, 885–887 (2011).
17. G. Zheng *et al.*, ALKBH5 is a mammalian RNA demethylase that impacts RNA metabolism and mouse fertility. *Mol. Cell* **49**, 18–29 (2013).
18. S. Zhong *et al.*, MTA is an Arabidopsis messenger RNA adenosine methylase and interacts with a homolog of a sex-specific splicing factor. *Plant Cell* **20**, 1278–1288 (2008).
19. L. Shen *et al.*, N(6)-Methyladenosine RNA modification regulates shoot stem cell fate in Arabidopsis. *Dev. Cell* **38**, 186–200 (2016).
20. K. Růžička *et al.*, Identification of factors required for m^6 A mRNA methylation in Arabidopsis reveals a role for the conserved E3 ubiquitin ligase HAKAI. *New Phytol.* **215**, 157–172 (2017).
21. L.-H. Wei *et al.*, The m^{6}A reader ECT2 controls trichome morphology by affecting mRNA stability in Arabidopsis. *Plant Cell* **30**, 968–985 (2018).
22. L. Arribas-Hernández *et al.*, An m^{6}A-YTH module controls developmental timing and morphogenesis in Arabidopsis. *Plant Cell* **30**, 952–967 (2018).
23. J. Scutenaire *et al.*, The YTH domain protein ECT2 is an m6A reader required for normal trichome branching in Arabidopsis. *Plant Cell* **30**, 986–1005 (2018).
24. H.C. Duan *et al.*, ALKBH10B is An RNA N6-methyladenosine demethylase affecting arabidopsis floral transition. *Plant Cell* **29**, 2995–3011 (2017).
25. M. Martínez-Pérez *et al.*, *Arabidopsis* m^{6}A demethylase activity modulates viral infection of a plant virus and the m^{6}A abundance in its genomic RNAs. *Proc. Natl. Acad. Sci. U.S.A.* **114**, 10755–10760 (2017).
26. Z. Bodi *et al.*, Adenosine methylation in Arabidopsis mRNA is associated with the 3′ end and reduced levels cause developmental defects. *Front. Plant Sci.* **3**, 48 (2012).
27. X. Chen, MicroRNA biogenesis and function in plants. *FEBS Lett.* **579**, 5923–5931 (2005).
28. C. R. Alarcón, H. Lee, H. Goodarzi, N. Halberg, S. F. Tavazoie, N6-methyladenosine marks primary microRNAs for processing. *Nature* **519**, 482–485 (2015).
29. C. R. Alarcón *et al.*, HNRNPA2B1 is a mediator of m(6)A-dependent nuclear RNA processing events. *Cell* **162**, 1299–1308 (2015).
30. A. Zielezinski *et al.*, mirEX 2.0—An integrated environment for expression profiling of plant microRNAs. *BMC Plant Biol.* **15**, 144 (2015).
31. D. Bielewicz *et al.*, mirEX: A platform for comparative exploration of plant pri-miRNA expression data. *Nucleic Acids Res.* **40**, D191–D197 (2012).
32. D. Dominissini *et al.*, Topology of the human and mouse m^{6}A RNA methylomes revealed by m^{6}A-seq. *Nature* **485**, 201–206 (2012).
33. S. J. Anderson *et al.*, N^6-Methyladenosine inhibits local ribonucleolytic cleavage to stabilize mRNAs in Arabidopsis. *Cell Rep.* **25**, 1146–1157.e3 (2018).
34. B. Szarzynska *et al.*, Gene structures and processing of Arabidopsis thaliana HYL1-dependent pri-miRNAs. *Nucleic Acids Res.* **37**, 3083–3093 (2009).
35. N. Liu *et al.*, N(6)-methyladenosine-dependent RNA structural switches regulate RNA-protein interactions. *Nature* **518**, 560–564 (2015).
36. C. Roost *et al.*, Structure and thermodynamics of N6-methyladenosine in RNA: A spring-loaded base modification. *J. Am. Chem. Soc.* **137**, 2107–2115 (2015).
37. N. Liu *et al.*, N6-methyladenosine alters RNA structure to regulate binding of a low-complexity protein. *Nucleic Acids Res.* **45**, 6051–6063 (2017).
38. F. Li *et al.*, Global analysis of RNA secondary structure in two metazoans. *Cell Rep.* **1**, 69–82 (2012).
39. S. J. Gosai *et al.*, Global analysis of the RNA-protein interaction and RNA secondary structure landscapes of the Arabidopsis nucleus. *Mol. Cell* **57**, 376–388 (2015).
40. S. J. Anderson, M. R. Willmann, B. D. Gregory, Protein interaction profile sequencing (PIP-seq) in plants. *Curr. Protoc. Plant Biol.* **1**, 163–183 (2016).
41. F. Vazquez, V. Gasciolli, P. Crété, H. Vaucheret, The nuclear dsRNA binding protein HYL1 is required for microRNA accumulation and plant development, but not post-transcriptional transgene silencing. *Curr. Biol.* **14**, 346–351 (2004).
42. M. H. Han, S. Goud, L. Song, N. Fedoroff, The *Arabidopsis* double-stranded RNA-binding protein HYL1 plays a role in microRNA-mediated gene regulation. *Proc. Natl. Acad. Sci. U.S.A.* **101**, 1093–1098 (2004).
43. Y. Kurihara, Y. Takashi, Y. Watanabe, The interaction between DCL1 and HYL1 is important for efficient and precise processing of pri-miRNA in plant microRNA biogenesis. *RNA* **12**, 206–212 (2006).
44. L. Song, M.-H. Han, J. Lesicka, N. Fedoroff, Arabidopsis primary microRNA processing proteins HYL1 and DCL1 define a nuclear body distinct from the Cajal body. *Proc. Natl. Acad. Sci. U.S.A.* **104**, 5437–5442 (2007).
45. L. Yang, Z. Liu, F. Lu, A. Dong, H. Huang, SERRATE is a novel nuclear regulator in primary microRNA processing in Arabidopsis. *Plant J.* **47**, 841–850 (2006).
46. G. Ren *et al.*, Regulation of miRNA abundance by RNA binding protein TOUGH in Arabidopsis. *Proc. Natl. Acad. Sci. U.S.A.* **109**, 12817–12821 (2012).
47. S. Ke *et al.*, m^{6}A mRNA modifications are deposited in nascent pre-mRNA and are not required for splicing but do specify cytoplasmic turnover. *Genes Dev.* **31**, 990–1006 (2017).

48. B. Molinie *et al*., m(6)A-LAIC-seq reveals the census and complexity of the m(6)A epitranscriptome. *Nat. Methods* **13**, 692–698 (2016).
49. S. D. Kasowitz *et al*., Nuclear m^6A reader YTHDC1 regulates alternative polyadenylation and splicing during mouse oocyte development. *PLoS Genet.* **14**, e1007412 (2018).
50. B. Slobodin *et al*., Transcription impacts the efficiency of mRNA translation via co-transcriptional N6-adenosine methylation. *Cell* **169**, 326–337.e12 (2017).
51. D. Windels *et al*., miR393 is required for production of proper auxin signalling outputs. *PLoS One* **9**, e95972 (2014).
52. P. Wang, K. A. Doxtader, Y. Nam, Structural basis for cooperative function of Mettl3 and Mettl14 methyltransferases. *Mol. Cell* **63**, 306–317 (2016).
53. Z. Yang, Y. W. Ebright, B. Yu, X. Chen, HEN1 recognizes 21-24 nt small RNA duplexes and deposits a methyl group onto the 2′ OH of the 3′ terminal nucleotide. *Nucleic Acids Res.* **34**, 667–675 (2006).
54. W. Park, J. Li, R. Song, J. Messing, X. Chen, CARPEL FACTORY, a Dicer homolog, and HEN1, a novel protein, act in microRNA metabolism in Arabidopsis thaliana. *Curr. Biol.* **12**, 1484–1495 (2002).
55. S. Nechaev, K. Adelman, Pol II waiting in the starting gates: Regulating the transition from transcription initiation into productive elongation. *Biochim. Biophys. Acta* **1809**, 34–45 (2011).
56. D. Bielewicz *et al*., Introns of plant pri-miRNAs enhance miRNA biogenesis. *EMBO Rep.* **14**, 622–628 (2013).
57. R. Schwab, C. Speth, S. Laubinger, O. Voinnet, Enhanced microRNA accumulation through stemloop-adjacent introns. *EMBO Rep.* **14**, 615–621 (2013).
58. J. Dolata *et al*., Salt stress reveals a new role for ARGONAUTE1 in miRNA biogenesis at the transcriptional and posttranscriptional levels. *Plant Physiol.* **172**, 297–312 (2016).
59. Z. Wang *et al*., SWI2/SNF2 ATPase CHR2 remodels pri-miRNAs via Serrate to impede miRNA production. *Nature* **557**, 516–521 (2018).
60. M. Bajczyk *et al*., SERRATE interacts with the nuclear exosome targeting (NEXT) complex to degrade primary miRNA precursors in Arabidopsis. *Nucleic Acids Res.* **48**, 6839–6854 (2020).
61. Z. H. Chen *et al*., Regulation of auxin response by miR393-targeted transport inhibitor response protein 1 is involved in normal development in Arabidopsis. *Plant Mol. Biol.* **77**, 619–629 (2011).
62. A. Si-Ammour *et al*., miR393 and secondary siRNAs regulate expression of the TIR1/AFB2 auxin receptor clade and auxin-related development of Arabidopsis leaves. *Plant Physiol.* **157**, 683–691 (2011).
63. K. D. Raczynska *et al*., The SERRATE protein is involved in alternative splicing in Arabidopsis thaliana. *Nucleic Acids Res.* **42**, 1224–1244 (2014).
64. F. Pontvianne *et al*., Identification of nucleolus-associated chromatin domains reveals a role for the nucleolus in 3D organization of the *A. thaliana* genome. *Cell Rep.* **16**, 1574–1587 (2016).
65. K. Knop *et al*., Active 5′ splice sites regulate the biogenesis efficiency of Arabidopsis microRNAs derived from intron-containing genes. *Nucleic Acids Res.* **45**, 2757–2775 (2017).
66. K. Kruszka *et al*., Developmentally regulated expression and complex processing of barley pri-microRNAs. *BMC Genomics* **14**, 34 (2013).